Hindawi
Advances in Civil Engineering
Volume 2018, Article ID 2492350, 10 pages
https://doi.org/10.1155/2018/2492350

Research Article

Numerical Analysis of the Degradation Characteristics of Bearing Capacity of a Corroded Reinforced Concrete Beam

Guifeng Zhao,[1] **Jiankun Xu**,[1] **Yaoliang Li**,[1,2] **and Meng Zhang**[1]

[1]*School of Civil Engineering, Zhengzhou University, Zhengzhou 450001, China*
[2]*Liuzhou Administration of Power Supply of Guangxi Grid Company, China Southern Power Grid, Liuzhou 545005, China*

Correspondence should be addressed to Meng Zhang; zhangmeng@zzu.edu.cn

Received 26 December 2017; Accepted 11 February 2018; Published 2 May 2018

Academic Editor: Song Han

The static load carrying capacity of a noncorroded reinforced concrete (RC) simply supported beam is numerically simulated by ABAQUS software, and the reliability of the finite element model is verified by comparing with the test results. Based on the above model, the macroscopic mechanical properties of the beam under different degrees of corrosion are calculated. In the calculation, the degradation of the bond-slip performance and mechanical properties of corroded rebars and the coupling effect on the bearing capacity and ductility degradation of the beams are considered. The results show that, under conditions of slight corrosion, the degradation of bond-slip performance between the rebar and concrete has no significant influence on the bearing capacity of the beam, while the degradation of the corroded rebar had a significant effect. Under moderate and severe corrosion conditions, the bearing capacity and ductility degradation caused by bond-slip are dominant in the mechanical property degradation of the beam. Overall, the macroscopic mechanical properties of the corroded beam are influenced by the coupling effect of bond-slip degradation and the mechanical property degradation of the rebar. With the increase in the corrosion rate, the bearing capacity and ductility of the beam are decreased, and its brittleness is increased.

1. Introduction

Among all kinds of civil engineering structures, the reinforced concrete structure is one of the most widely used structural forms. With the increase of service life, the materials of the reinforced concrete structure will degrade under the direct or indirect influence of corrosive media from the outside world, resulting in durable damage (such as surface cracks, carbonization, spalling, and corrosion of rebars). Accidents causing damage to concrete structures often occur in the case of damage resulting in durability damage, and the resulting loss is even more difficult to measure. The sum of the annual maintenance, repair, and reinforcement costs for corrosion of reinforced concrete structures in the world has exceeded 100 billion dollars [1]. According to statistics, among the many factors leading to the damage of the durability of a reinforced concrete structure, rebar corrosion is the most common. Once the rebar in the concrete is corroded, the corrosion rate of the steel is further increased. Corrosion will lead to the degradation of the geometric parameters of steel and mechanical properties, mainly reflected in the following [2–4]: (1) loss of mass and effective cross-sectional area; (2) the decline of nominal yield stress and ultimate stress; (3) the decrease of the nominal elongation rate and ultimate strain; and (4) the degradation of bond-slip. Degradation of these properties will inevitably weaken the static bearing capacity of the structure to a certain extent and increase its brittleness. Therefore, it is of great theoretical significance and practical engineering value to study the degradation characteristics of the bearing capacity of concrete structures or members caused by corrosion of rebars.

The previous research on the corrosion direction of RC members mainly focuses on two aspects, which are anticorrosion capability of the members and the mechanical properties of the corroded members [2–4]. Most of the anticorrosive researches of RC members are to add some additional materials (such as polypropylene fiber [5–9], silica fume, and

nanomaterial [10]), or some mechanical treatment schemes for members are adopted to reduce the effect of corrosion.

At present, noncorroded RC frame structure has been widely studied in engineering [11–14]. However, there are relatively few studies on corroded RC structures or members affected by corrosion. The existing research focuses on the macroscopic mechanical properties of steel corrosion members. In most natural environments, the corrosion and degradation of reinforced concrete members will take a long time. If it is simulated under natural conditions, it will take a lot of time and cost [13]. Therefore, the methods of changing the temperature, concentration, and composition of the corrosive medium are used to accelerate the corrosion of the components during the test [14, 15], and some scholars also accelerate the simulation process by the method of external current. In order to get enough test data, a lot of samples are needed for the accelerated corrosion test. In addition, the preparation of test specimens and related corrosion media will also cost a lot of time and cost [16–18], and there is few relevant impact parameters that can be used for reference during the course of experiment. Through a long period of study, it is found that the methods mentioned above are less similar to the actual corrosion in the natural environment. Based on these restrictions, the performance of corroded reinforced concrete members has not been fully studied.

With the rapid development of computer technology, numerical simulation has been widely used in engineering [19]. Moreover, numerical simulation presents numerous advantages such as short computation time and low cost, and it considers the influences of various parameters. In this paper, the characteristics of the degradation of bearing capacity of reinforced concrete simply supported beams before and after corrosion were studied using ABAQUS software to provide a reference for the performance evaluation and maintenance and reinforcement of rust structures or members.

2. Constitutive Relationship of Corroded Reinforced Concrete

In this paper, the concrete-damaged plasticity model (CDP model) in ABAQUS is used to simulate the mechanical behaviour of concrete materials [20]. The elastoplastic model of the double inclined line is used to simulate the stress-strain relationship of rebar material. The nonlinear spring (SPRING2) is used to simulate the bond-slip between the rebar and the concrete.

2.1. Constitutive Relationship of Concrete. The CDP model is a constitutive relation model for concrete in the implicit algorithm of ABAQUS software. The model was first proposed by Lubliner et al. [21] and improved by Lee and Fenves [22]. The model can automatically consider the biaxial or three-axis stress state of the material unit and calculate the degradation in the materials during stress under the condition of only inputting uniaxial stress-strain parameters and damage parameters of the material. Therefore, the model can reflect the mechanical response of the material more truthfully in the process of monotonic loading and repeated loading/unloading [4].

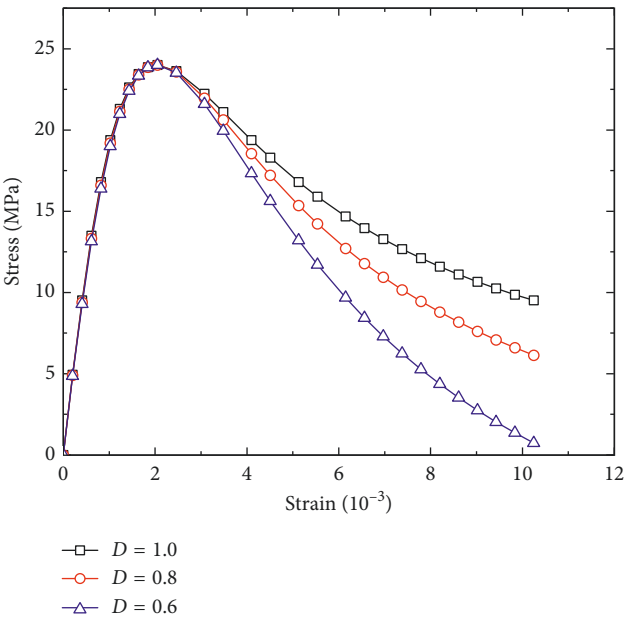

Figure 1: The compressive model of Sargin.

2.1.1. Stress-Strain Relationship of Concrete Material. Because the mechanical properties of concrete materials have strong randomness characteristics [23, 24], this paper adopts the Sargin model [25] with adjustable descent velocity to define the compressive stress-strain relationship (Formula (1) and Figure 1). The Arab model [26] is used to define the tensile stress-strain relationship of concrete (Formula (2) and Figure 2).

The compressive model of Sargin:

$$\sigma_c = \frac{\left(\left(E_c/E_g\right)\left(\varepsilon/\varepsilon_c\right)\right) + (D-1)\left(\varepsilon/\varepsilon_c\right)^2}{1 + \left(\left(E_c/E_g\right) - 2\right)\left(\varepsilon/\varepsilon_c\right) + D\left(\varepsilon/\varepsilon_c\right)^2} f_c, \quad (1)$$

$$E_g = \frac{f_c}{\varepsilon_c},$$

where E_c is the initial elastic modulus of concrete, with data selected from [27]; E_g is the secant modulus of concrete; and ε_c is the strain corresponding to the peak stress of concrete. In this paper, a strain value of 0.0020 is used; f_c is the peak stress of concrete, and D is the adjustment parameter of the resist compression softening section of concrete; $0 < D < 1$.

The tensile model of Arab:

$$\sigma_t = \begin{cases} y f_t, & y \le 1 \\ \left(\dfrac{\beta y f_t}{\beta - 1 + y^\beta}\right), & y \ge 1, \end{cases} \quad (2)$$

$$y = \frac{\varepsilon}{\varepsilon_t},$$

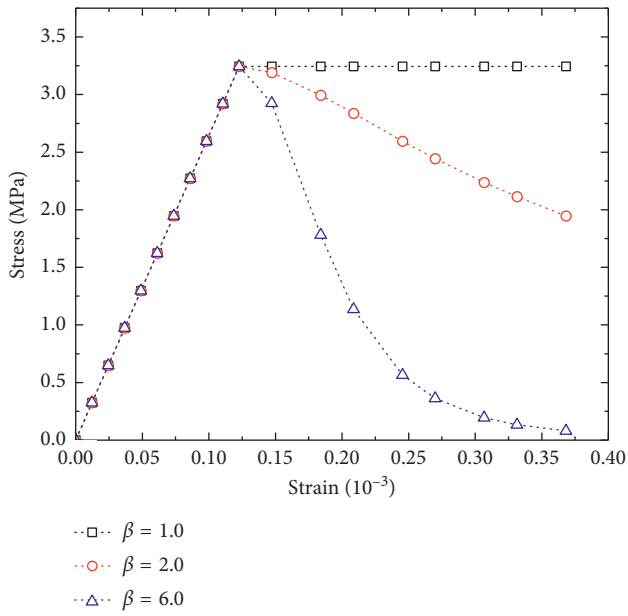

Figure 2: The tensile model of Arab.

where f_t is the tensile strength of concrete, with data selected from [28]; ε_t is the tensile peak strain of concrete, which can be approximated to $\varepsilon_t = f_t/E_c$; and β is the adjustment parameter of the resist tensile softening section of concrete; $\beta > 1$.

To fit the test results [29], the damage characteristics of concrete materials (3) are defined by the Lee and Fenves damage parameter model [30] with ABAQUS, which makes the calculation results closer to the experimental results:

$$d = 1 - \frac{\sigma_{\text{true}} E_c^{-1}}{\varepsilon^{\text{pl}}\left(1/b_{c/t} - 1\right) + \sigma_{\text{true}} E_c^{-1}},$$

$$\varepsilon_{\text{true}} = \ln(1 + \varepsilon),$$

$$\sigma_{\text{true}} = \sigma(1 + \varepsilon), \tag{3}$$

$$\varepsilon^{\text{in}} = \varepsilon_{\text{true}} - \frac{\sigma_{\text{true}}}{E_c},$$

$$\varepsilon^{\text{pl}} = b_{c/t}\varepsilon^{\text{in}},$$

where d is the tensile/pressure damage factor of concrete; σ_{true} is the true stress; ε^{pl} is the plastic strain in the concrete; $\varepsilon_{\text{true}}$ is the real strain of concrete; ε^{in} is the inelastic strain in the concrete; and $b_{c/t}$ is the scale factor between plastic strain and inelastic strain. In this paper, the tension $b_{c/t}$ was 0.3, and the pressure $b_{c/t}$ was 0.7 during calculation.

Corrosion will result in the degradation of the material property of the concrete cover. In a service environment, chloride ions penetrate the surface of the rebar through the primary fractures or cracks of the concrete cover, form a conductive medium on the surface of the rebar, and participate in primary cell reflection of the corroded rebar [31, 32]. In the rebar corrosion state, the cracks of the concrete cover produce the stress concentration due to the extrusion force of the corroded rebar, which further increases the crack width, causing cracking and spalling. The degree and location of the cracking and exfoliation of the concrete cover have a strong randomness. To date, this process is still difficult to describe with a precise mechanical model. In this paper, the simplified formula recommended in [33, 34] is used for calculation as follows:

$$f_{c-cor} = \frac{f_c}{1 + \gamma\left(\varepsilon_{t-cor}/\varepsilon_c\right)},$$

$$\varepsilon_{t-cor} = \frac{b_{cor} - b}{b},$$

$$b_{cor} = b + n\omega_{cor}, \tag{4}$$

$$\omega_{cor} = \sum_i u_{icor} = 2\pi\left(\upsilon_{cor} - 1\right)\text{X},$$

$$\rho_s = \frac{2\text{X}}{r} - \left(\frac{\text{X}}{r}\right)^2,$$

where f_{c-cor} is the compressive peak strength of corroded concrete; γ is the correlation coefficient between the surface shape of the rebar and its diameter, assuming 0.1; ε_{t-cor} is the cracked strain of the generalized concrete; b is the primitive width of the member; b_{cor} is the width of the cross section of the corroded member; n is the number of compressive longitudinal tendons of corrosion damage; ω_{cor} is the total width of the corrosion crack; υ_{cor} is the proportion coefficient of the oxidation product of corroded rebar and the volume before the corrosion of the rebar, 2.0; u_{icor} is the crack width of the corrosion member of number i; X is the corrosion depth of the rebar; ρ_s is the loss rate of corrosion of the rebar cross section; r is the radius before the corrosion of the rebar; and the weighted mean value is used when the diameter of the rebar is different.

2.2. Constitutive Relationship of Rebar and Degradation of Corrosion Mechanical Properties. In this paper, the constitutive relationship of the rebar material is simulated by using a double-fold linear elastoplastic strengthening model (Figure 3). The model can fully reflect the reinforcement behaviour after the rebar yield, so it is widely used in the static analysis of the structure.

There are two main forms of rebar corrosion [35–37]: (1) uniform corrosion and (2) pit corrosion. The characteristic of uniform corrosion is that the section size and shape of the rebar do not change along the longitudinal direction of the rebar, and this state is a perfect state. However, the pit corrosion is a common phenomenon in the test room or in the state of natural corrosion due to the randomness of the size and distribution of primary cracks and voids in the corrosion process of the rebar, which will cause local concentrations of chloride ions, electrons, and random pitting corrosion on the surface of the corroded rebar because the real stress, strain, and other parameters of the steel bar are

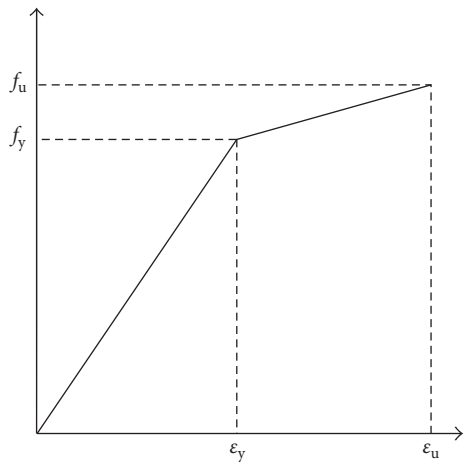

Figure 3: Constitutive relations of steel bars.

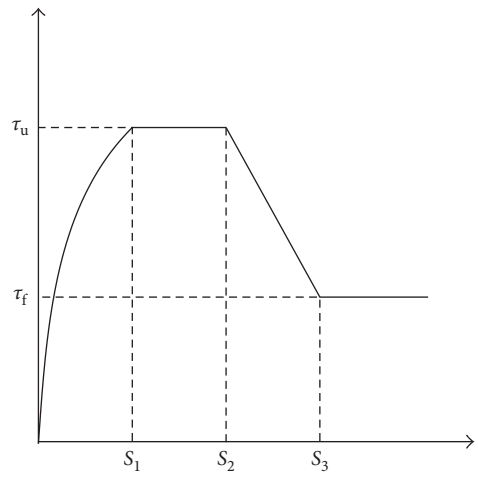

Figure 4: The diagram of the CEB-FIB bond-slip model.

not changed under corrosion conditions. Therefore, for the uniform corrosion, the corrosion state of the rebar can be simulated directly by the direct reduction of the section area of the rebar. However, the state of pit corrosion, considering the randomness of pit corrosion distribution, is very difficult to simulate directly using finite element software [38]. Therefore, we used the equivalent uniform corrosion state to simulate the pit corrosion rebar.

The Wang and Liu model [39] can be used in the nominal yield strength and nominal elastic modulus of the corroded rebar after pit corrosion:

$$\begin{aligned} f_{yc} &= (1 - 0.00198\delta) f_y, \\ E_{sc} &= (1 - 0.00113\delta) E_s, \end{aligned} \tag{5}$$

where f_y is the nominal yield strength of the rebar before corrosion; f_{yc} is the nominal yield strength of the rebar after corrosion; E_s is the nominal elastic modulus of the rebar before corrosion; E_{sc} is the nominal elastic modulus of the rebar after corrosion; and δ is the mass loss rate of the corroded rebar, and the transformation relationship between mass loss rate of the corroded rebar and the cross-sectional loss rate can be seen in the following equation [39]:

$$\rho_s = \begin{cases} 0.013 + 0.987\delta, & \delta \le 10\% \\ 0.061 + 0.939\delta, & 10\% < \delta \le 20\% \\ 0.129 + 0.871\delta, & 20\% < \delta \le 30\% \\ 0.199 + 0.810\delta, & 30\% < \delta \le 40\%. \end{cases} \tag{6}$$

For the ultimate strength and ultimate strain of the pit corrosion rebar, we use the fuzzy formula of Wu and Yuan [2] to calculate as follows:

$$\begin{aligned} f_{uc} &= (1.0 - 0.019\delta) f_u, \\ \varepsilon_{uc} &= (1.0 - 0.021\delta) \varepsilon_u, \end{aligned} \tag{7}$$

where f_{uc} is the nominal ultimate strength of the rebar after corrosion and ε_{uc} is the nominal ultimate strain of the rebar before corrosion.

2.3. Constitutive Relationship of Bond-Slip. The reason why the two parts of the rebar and concrete materials can better display their respective advantages is a good bond-slip relationship between rebar and concrete, which can fully coordinate the deformation of the rebar and concrete to achieve the purpose of coordination of deformation [40].

ABAQUS finite element software uses the single-axis tension and pressure function of the nonlinear spring (SPRING2) to simulate the bond-slip behaviour of the rebar and concrete. The model concentrates the slip shear stress on the surface of the rebar to the nonlinear spring element, and the relative dislocation between the rebar and the concrete is completed by pulling the rebar through the deformation of the spring [41]. The mechanics calculation formula of the nonlinear spring element is

$$\begin{aligned} F_i &= A_i \times \tau, \\ A_i &= 2\pi R l, \end{aligned} \tag{8}$$

where F_i is the axial force of a single spring unit; A_i is interaction area of a single spring unit; τ is the shear stress on the surface of the rebar; R is the radius of a single rebar at the linkage unit; and l is the spacing of the adjacent spring element.

Through the research and analysis of the uniaxial tensile test curve of the corroded rebar in the literature [42], the shear stress displacement curve of the corroded rebar is found to be similar to the shear stress displacement curve defined by the European Standard CEB-FIB [43]. Therefore, the shear stress parameter of CEB-FIB definition (8) is adopted in this paper, and the bond-slip model of the corroded rebar is obtained by modifying the key point parameters of the curve (formula (9) and Figure 4):

$$\tau = \begin{cases} \tau_u (s/s_1)^{\alpha}, & 0 < s \le s_1 \\ \tau_u, & s_1 < s \le s_2 \\ \tau_u - (\tau_u - \tau_f)\left((s - s_2)/(s_3 - s_2)\right), & s_2 < s \le s_3 \\ \tau_f, & s_3 < s, \end{cases} \tag{9}$$

Table 1: The parameters of the CEB-FIP bond-slip model.

s_1	s_2	s_3	α	τ_u	τ_f
1.0 mm	3.0 mm	Rib spacing	0.4	$2.5\sqrt{f_c}$	$0.4\tau_u$

Table 2: The material parameters of concrete.

Material	E_c (MPa)	f_c (MPa)	f_t (MPa)
Concrete	29509.97	34.55	2.97

where τ_u is the maximum shear stress; s is the value of the displacement; τ_f is the minimum shear stress; and α is the exponent of upward section of the curve. The values of each parameter in (9) are shown in Table 1.

The reduction coefficient of the shear stress peak value of the corroded rebar [36] can be calculated by the following equation:

$$\theta = \frac{\tau_u^{cor}}{\tau_u} = 0.9959e^{0.0041\delta} + 0.0069e^{0.7858\delta}, \delta \le 4\%$$
$$\theta = \frac{\tau_u^{cor}}{\tau_u} = 9.662e^{-0.5552\delta} + 0.1887e^{0.0069\delta}, \delta > 4\%. \quad (10)$$

Because the stirrup has the effect of pulling, the slip shear stress will not be reduced to the numerical point with the increase of the slip displacement. After the corrosion, the shear stress parameter τ_f will also change accordingly. Almusallam [44], Auyeung et al. [45], and other scholars believe that the final value of the longitudinal rebar corrosion τ_f is 0.15 times τ_u. Therefore, in this paper, the research conclusions of Almusallam [44] and Auyeung et al. [45] are cited to correct corroded τ_f.

3. The Establishment and Reliability Verification of the Finite Element Model of an Uncorroded RC Simply Supported Beam

To establish a more credible finite element analysis model, we first take a simply supported RC beam without corrosion as an example. The finite element analysis is carried out and compared with the test results to verify the reliability of the finite element model. On this basis, the bearing capacity of the simply supported RC beam with different corrosion degrees is analysed.

3.1. Introduction of Test Beam Model. The model of the test beam is from the literature [29], and the beam number is LA6. The total length of the test beam is 2400 mm, and the spacing of the support is 2100 mm. The distribution beam applies the load to the two points at the point of trisection of the top of the beam. The section size of the beam is 200 mm × 300 mm, and the depth of the concrete cover is 25 mm. The bottom of the beam is configured with two diameters of the 20 mm HRB335 and one diameter of the 12 mm HPB235 longitudinal rebars. The top of the beam is configured with two diameters of the 12 mm HPB235

Table 3: The material parameters of rebars.

Type of rebar	E_s (MPa)	f_y (MPa)	f_u (MPa)	ε_u
HPB235	210000	258.25	393.39	0.15
HRB235	200000	373.71	578.28	0.15

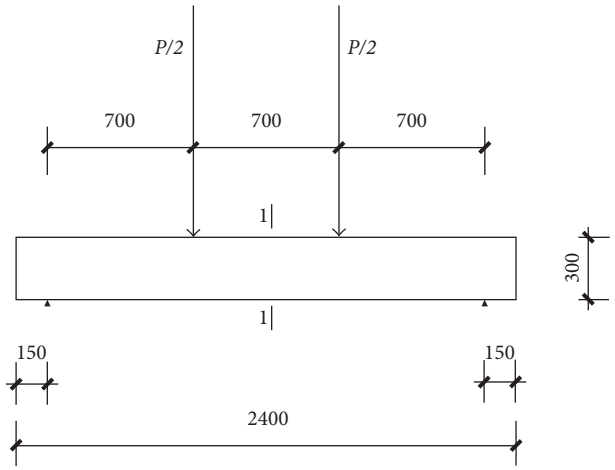

Figure 5: Diagram of the beam size.

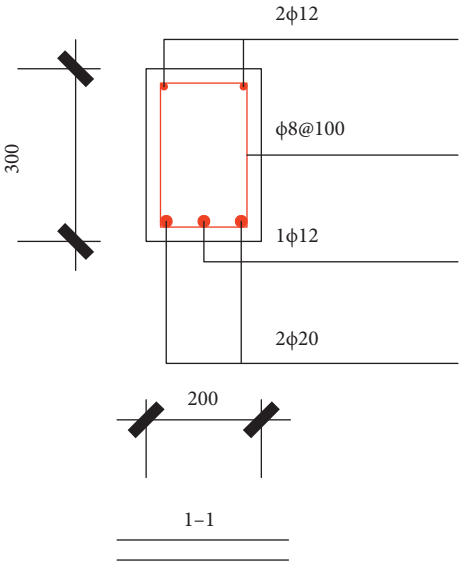

Figure 6: The reinforcement of beam section.

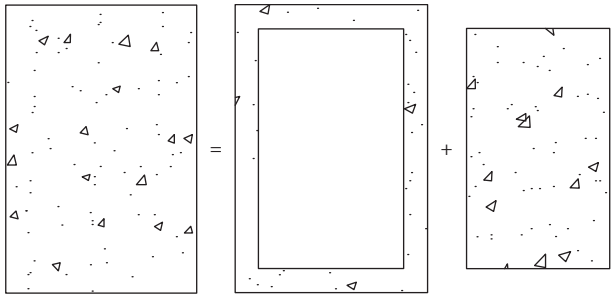

Figure 7: Finite element analysis of concrete section.

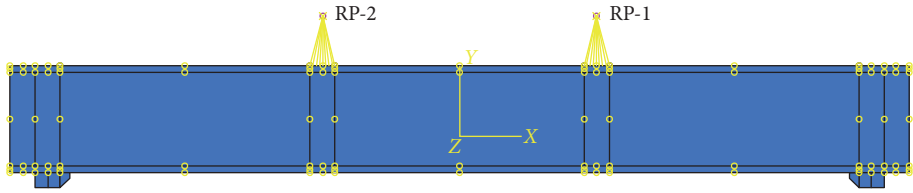

Figure 8: Finite element analysis model.

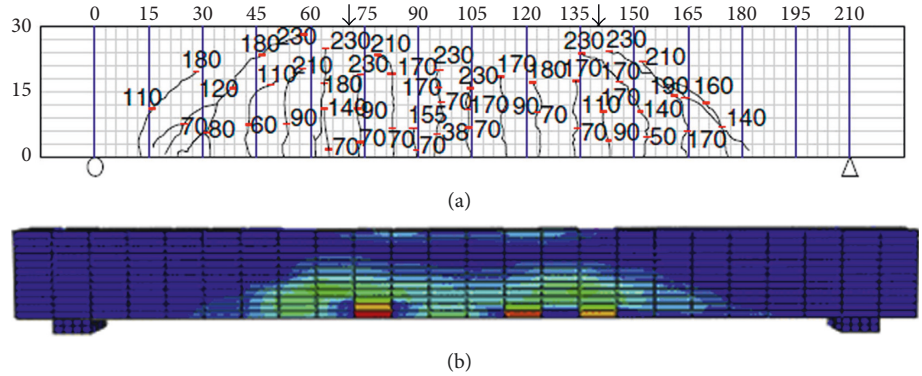

Figure 9: Comparison of (a) test model and (b) finite element model in cracking distribution.

longitudinal rebar. The stirrup is the HPB235 rebar of 8 mm diameter; the stirrup is two limbs, and the distance is 100 mm. The measured strength of concrete is 34.55 MPa. The parameters of tensile strength and elastic modulus of elasticity of concrete are shown in Table 2, and the parameters of rebar properties are shown in Table 3. The diagrams of geometric parameters and rebar parameters are shown in Figures 5 and 6, respectively.

3.2. The Establishment of a Finite Element Model. The C3D8R element is used to simulate concrete (unit size is 25 mm × 25 mm × 100 mm). The T3D2 element is used to simulate the rebar (unit length is 100 mm). The SPRING2 element is used as the bonding element (the unit is a nonlength unit). Because the rebar is only comparatively remarkable in the longitudinal slip, the SPRING2 element nonlinearity is defined only in the longitudinal direction of the beam in this paper. The slip of the rebar is not considered in the lateral and high directions of the beam, and the spring stiffness in this direction is defined as 2×10^{12} N/mm.

According to the weakening rule of concrete cover defined by (4), the block modelling technology is used to peel off the concrete cover from the core concrete (Figure 7), but it does not change the force and displacement transfer between nodes. To facilitate the convergence of models, two reference points (RP1 and RP2) are set up at the loading point of the beam. The distribution of the reference points and the top surface of the beam are constrained by the distributed coupling mode, and then the symmetrical displacement load is applied at the loading point. To prevent the stress concentration in the loading process, two rigid cushion plates are set up at the support, and the bottom plate

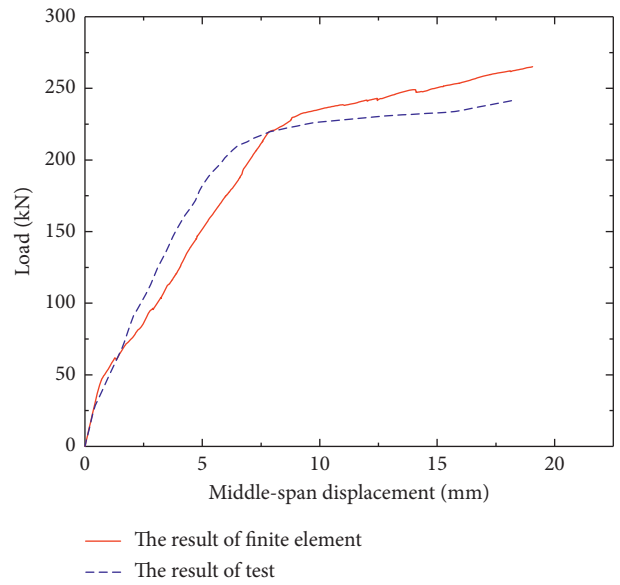

Figure 10: Comparison of load and displacement curves between test model and finite element model.

and the bottom of the beam are restrained by the binding (tie) mode. The finite element model is shown in Figure 8.

3.3. Reliability Verification of the Finite Element Model. Figure 9 shows the distribution of cracks after loading of the beams that are not corroded. The distribution of the cracks produced by the results of the finite element analysis is basically consistent with the distribution of the cracks in the test. On the whole, the cracks are symmetrical in the cross section and are distributed in a double arch.

Table 4: Comparison of key point mechanical parameters.

Item	Crack load (kN)	Yield load (kN)	Ultimate load (kN)	Ultimate displacement (mm)
Results of test (a)	40	210.2	241.4	18.2
Results of numerical (b)	42.2	220.6	264.8	19.1
Relative error (%) $(((b)-(a))/(a))\times 100\%$	5.5	4.9	9.7	4.9

Table 5: The strength of the concrete cover of the corroded member.

Corrosion rate of rebar section	0%	5%	10%	15%
Concrete compressive (MPa)	34.55	17.37	11.08	8.61

Table 6: Mechanical parameters of corroded rebars.

Corrosion rate of rebar section	E_s (MPa)	f_y (MPa)	f_u (MPa)	ε_u (MPa)
		Diameter of rebar $D = 12$ mm		
0%	210000	258.25	393.39	0.15
5%	197769.7	231.90	354.87	0.13
10%	185829.1	206.17	317.26	0.12
15%	172889.8	178.28	276.50	0.10
		Diameter of rebar $D = 20$ mm		
0%	200000	373.71	578.28	0.15
5%	188500.8	336.06	522.38	0.13
10%	176835.3	297.87	465.66	0.12
15%	164508.9	257.51	405.73	0.10

Table 7: The degradation of bonding stress.

Corrosion rate of rebar section	0%	5%	10%	15%
τ_u (MPa)	14.7	11.0	3.7	2.9
τ_f (MPa)	5.9	2.2	2.2	2.2

The load-deformation curves obtained by the finite element calculation and the test are shown in Figure 10 and Table 4. As shown in Figure 10, the finite element analysis result is very close to the test curve. The main difference is that the test model has greater stiffness, while its yield displacement and bearing capacity are relatively small. From the comparison in Table 4, the errors of all parameters are less than 10%, and all are within the acceptable range of error. The above results indicate that the finite element model established in this paper is reliable. Thus, the bearing capacity analysis of the corroded members can be further carried out based on this model.

4. Numerical Analysis of Bearing Performance of the Corroded Reinforced Concrete Simply Supported Beam

Considering that the bottom of the beam is more easily cracked under normal conditions, the chloride ion can corrode the bottom longitudinal reinforcement through a crack in the bottom. In this paper, the bearing capacity of the beam is mainly considered when the longitudinal reinforcement is corroded at the bottom of the beam.

The following 4 types of corrosion conditions are considered in the analysis: the corrosion rate distribution of the corresponding rebar section is 0% (noncorrosion), 5% (slight corrosion), 10% (medium corrosion), and 15% (severe corrosion). The parameters used in modelling of noncorrosion corrosions are exactly the same as the parameters of the previous finite element model.

The calculated parameters of the corroded member are shown in Tables 5–7 (the corrosion rates in the table are all the corrosion rates of the cross section).

In the following analysis, the degradation of bond-slip properties, the degradation of mechanical properties of the rebar, and the degradation law of macromechanical properties of the members caused by their coupling are considered. The load-displacement curves of the members with different corrosion rates under the above three conditions are shown in Figures 11–13.

Figure 11 shows that there is no significant effect on the degradation of the rebar-concrete bond-slip behaviour under slight corrosion. Under the medium corrosion condition, the degradation of the rebar-concrete bond-slip properties mainly affects the ductility of the member (deferring yield displacement and limiting the development of ultimate displacement). Under the severe corrosion condition, the degradation of bond-slip properties seriously restricts the exertion of the mechanical properties of the rebar and reduces the ductility and bearing capacity of members, resulting in brittle failure mechanism. The degradation of the

Table 8: The key point value of the load-displacement curve under coupling factors.

Corrosion rate of cross section	Yield load (a) (kN)	Yield displacement (b) (mm)	Ultimate load (c) (kN)	Ultimate displacement (d) (mm)	Ductility ratio, (c)/(d)
0%	220.6	8.0	264.8	19.1	2.39
5%	200.0	7.6	246.0	17.9	2.36
10%	173.8	7.2	203.8	16.5	2.29
15%	143.8	6.6	153.8	11.7	1.77

Table 9: Comparison of parameter lower rate and corrosion rate.

Corrosion rate of cross section	Reduction percentage of yield load (%)	Reduction percentage of yield displacement (%)	Reduction percentage of ultimate load (%)
0%	0	0	0
5%	9.3	5.0	7.1
10%	21.2	10.0	23.0
15%	34.8	17.5	41.9

Note: reduction percentage = (no corrosion index − corrosion index)/no corrosion index × 100%.

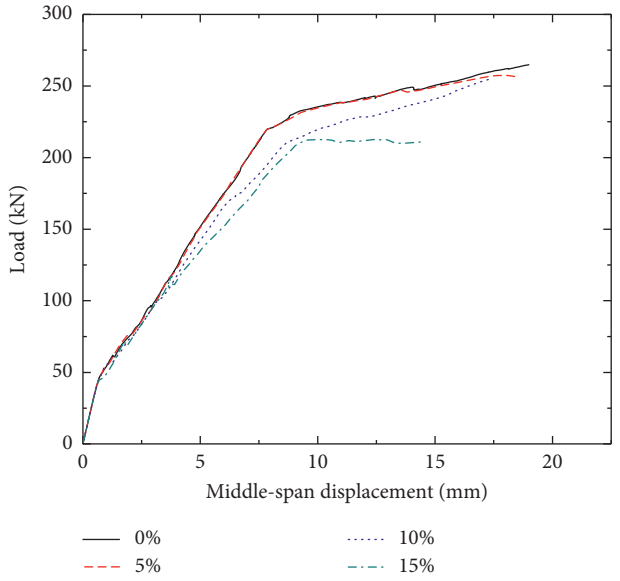

Figure 11: The load-displacement curve due to bonding degradation.

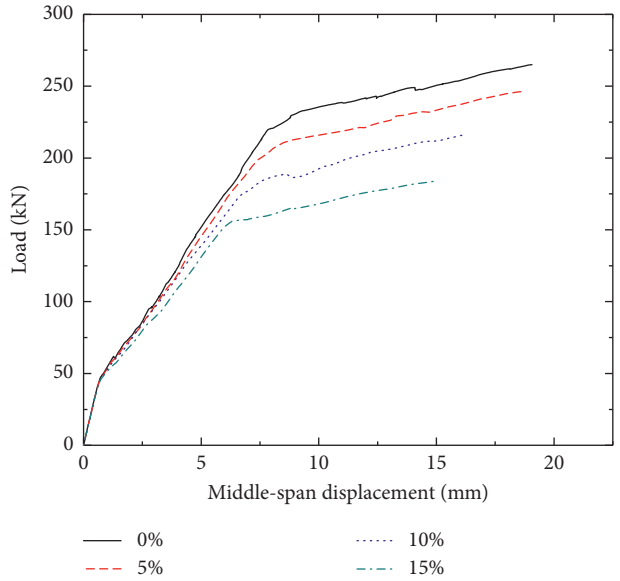

Figure 12: The load-displacement curve due to rebar mechanical property degradation.

bond-slip properties of the rebar caused by corrosion above the middle level has a great influence on the ductility development and the mechanical properties of the rebar.

The analysis of Figure 12 also shows that the bearing capacity and ductility (ultimate displacement/yield displacement) of members are gradually weakened with the increase of the corrosion rate, while the ductile failure mechanism still exists. The degradation of the mechanical properties of the rebar caused by corrosion directly affects the bearing capacity and ductility of the members, which is equivalent to decreasing the reinforcement ratio of the member section or decreasing the strength level of the reinforcement.

In Figure 13, the effects of the degradation of the bond-slip properties and the degradation of mechanical properties of the rebar are taken into consideration. The bearing capacity and characteristic displacement of the beam decrease gradually with the increase in the rebar corrosion rate, and the failure mode of the beams gradually develops to brittleness. Compared with Figure 12, the bearing capacity and ductility degradation speed of members are accelerated, indicating that the mechanical property degradation and the bond-slip property degradation caused by corrosion have a strong coupling effect. Under this coupling effect, the bearing capacity and ductility of the members decrease significantly with the increase of the corrosion rate of the rebar.

To further understand the change characteristics of the bearing behaviour of the members under the coupling action of the degradation of the mechanical properties and the degradation of the bond-slip performance, the key points of load-displacement curves in Figure 13 are listed in Table 8.

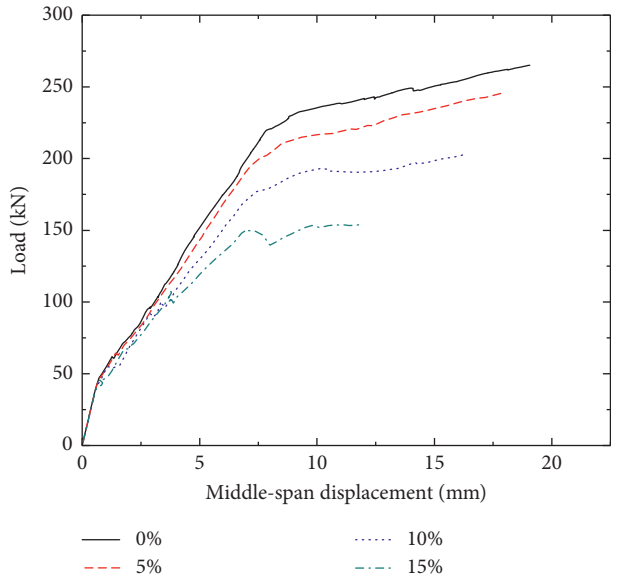

FIGURE 13: The load-displacement curve of beams due to corrosion.

According to the analysis of Table 8, the yield load/displacement, ultimate load/displacement, and ductility ratio of members are all decreased to some extent after rebar corrosion, and the decrease of yield load/displacement and ultimate load is obvious. Therefore, the relationship between the reduced ratio coefficient of the above three parameters (Table 9) and the corrosion rate of the rebar cross section can be fitted. The fitting results can be seen in the following equations:

$$I_{yc} = -0.00045 + 1.681\rho_s + 4.3\rho_s^2, \quad 5\% \le \rho_s \le 15\%, \quad (11)$$

$$\Delta_{yc} = -0.005 + 1.15\rho_s, \quad 5\% \le \rho_s \le 15\%, \quad (12)$$

$$I_{uc} = -0.0029 + 1.062\rho_s + 11.8\rho_s^2, \quad 5\% \le \rho_s \le 15\%, \quad (13)$$

where I_{yc} is the reduction percentage of the yield load; Δ_{yc} is the reduction percentage of the yield displacement; I_{uc} is the reduction percentage of the ultimate load; and ρ_s is the corrosion rate of the cross section.

5. Conclusions

In this paper, the bearing capacity and ductility degradation characteristics of a reinforced concrete simply supported beam with different corrosion rates are simulated and analysed. The main conclusions are as follows:

(1) Under slight corrosion conditions, the degradation of the bond-slip properties between rebar and concrete has no significant influence on the bearing capacity of the member, while the degradation of the mechanical properties of the rebar caused by corrosion has a great influence on the bearing capacity and ductility of the member.

(2) With the increase in the corrosion rate of the rebar, the bearing capacity and ductility of the member decreased significantly. Under moderate and severe corrosion conditions, the bearing capacity and ductility degradation of the member caused by the degradation of the bond-slip properties are dominant.

(3) On the whole, the bearing capacity of the member decreases with the increase of the rebar corrosion, and the failure mode develops from initial ductile failure to brittle failure, which is a disadvantage for the structure hit by an earthquake.

Conflicts of Interest

The authors declare that there are no conflicts of interest regarding the publication of this paper.

Acknowledgments

This research has been funded by the Outstanding Young Talent Research Fund of Zhengzhou University (Grant no. 1521322004), Guangdong Provincial Key Laboratory of Durability for Civil Engineering, Shenzhen University (Grant no. GDDCE 12-06), and Foundation for University Young Key Teacher by Henan Province (Grant no. 2015GGJS-151).

References

[1] P. A. Sadegh, C. Dehghanian, and A. Kosari, "Corrosion protection of the reinforcing steels in chloride-laden concrete environment through epoxy/polyaniline–camphorsulfonate nanocomposite coating," *Corrosion Science*, vol. 90, pp. 239–247, 2015.

[2] Q. Wu and Y. S. Yuan, "Experimental study on the deterioration of mechanical properties of corroded steel bars," *China Civil Engineering Journal*, vol. 41, no. 12, pp. 42–47, 2008.

[3] Y. F. Fan, Z. G. Huang, J. M. Li, and L. G. Guo, "Research on cohesive property between reinforcement and concrete of corroded RC member," *Industrial Construction*, vol. 29, pp. 49–51, 1999.

[4] G. F. Zhao, M. Zhang, Y. L. Li, and D. LI, "The hysteresis performance and restoring force model for corroded reinforced concrete frame columns," *Journal of Engineering*, vol. 2016, Article ID 7615385, 19 pages, 2016.

[5] P. Zhang, Q. F. Li, and H. Y. Zhang, "Combined effect of polypropylene fiber and silica fume on mechanical properties of concrete composite containing fly ash," *Journal of Reinforced Plastics and Composites*, vol. 30, no. 16, pp. 1349–1358, 2011.

[6] S. Han and J. Plank, "Mechanistic study on the effect of sulfate ions on polycarboxylate superplasticisers in cement," *Advances in Cement Research*, vol. 25, no. 4, pp. 200–207, 2013.

[7] N. Banthia and R. Gupta, "Influence of polypropylene fiber geometry on plastic shrinkage cracking in concrete," *Cement and Concrete Research*, vol. 36, no. 7, pp. 1263–1267, 2006.

[8] Z. Bayasi and J. Zeng, "Properties of polypropylene fiber reinforced concrete," *ACI Materials Journal*, vol. 90, no. 6, pp. 605–610, 1993.

[9] O. Karahan and C. D. Atis, "The durability properties of polypropylene fiber reinforced fly ash concrete," *Materials & Design*, vol. 32, no. 2, pp. 1044–1049, 2011.

[10] M. Safiuddin, M. Gonzalez, J. Cao, and S. L. Tighe, "State-of-the-art report on use of nano-materials in concrete," *International Journal of Pavement Engineering*, vol. 15, no. 10, pp. 940–949, 2014.

[11] Y. G. Du, L. A. Clark, and A. H. C. Chan, "Residual capacity of corroded reinforcing bars," *Magazine of Concrete Research*, vol. 57, no. 3, pp. 135–147, 2005.

[12] C. Jiang, Y. F. Wu, and M. J. Dai, "Degradation of steel-to-concrete bond due to corrosion," *Construction and Building Materials*, vol. 158, pp. 1073–1080, 2018.

[13] W. J. Zhu, R. Francois, C. P. Zhang, and D. L. Zhang, "Propagation of corrosion-induced cracks of the RC beam exposed to marine environment under sustained load for a period of 26 years," *Cement and Concrete Research*, vol. 103, pp. 66–76, 2018.

[14] S. B. Gao, J. Ni, D. X. Zhang, and H. B. Ge, "Strength degradation of reinforced concrete piers wrapped with steel plates under local corrosion," *Steel and Composite Structures*, vol. 24, no. 6, pp. 753–765, 2017.

[15] L. Abosrra, A. F. Ashour, and M. Youseffi, "Corrosion of steel reinforcement in concrete of different compressive strengths," *Construction and Building Materials*, vol. 25, no. 10, pp. 3915–3925, 2011.

[16] D. Coronelli, "Corrosion cracking and bond strength modeling for corroded bars in reinforced concrete," *ACI Structural Journal*, vol. 99, no. 3, pp. 267–276, 2002.

[17] T. Vidal, A. Castel, and R. Francois, "Analyzing crack width to predict corrosion in reinforced concrete," *Cement and Concrete Research*, vol. 34, no. 1, pp. 165–174, 2004.

[18] R. Zhang, A. Castel, and R. Francois, "The corrosion pattern of reinforcement and its influence on serviceability of reinforced concrete members in chloride environment," *Cement and Concrete Research*, vol. 39, no. 11, pp. 1077–1086, 2009.

[19] T. Pregartner, J. Cairns, and J. Ožbolt, "Modelling effect of corrosion on bond strength of plain bar reinforcement," *Structural Concrete*, vol. 5, no. 3, pp. 113–120, 2004.

[20] ABAQUS, *ABAQUS Theory Manual, Version 6.12*, Hibbitt, Carlsson, and Sorensen, Inc., Pawtucket, RI, USA, 2012.

[21] J. Lubliner, J. Oliver, S. Oller, and E. Õnate, "A plastic damage model for concrete," *International Journal of Solids and Structures*, vol. 25, no. 3, pp. 299–326, 1989.

[22] J. Lee and G. L. Fenves, "Plastic-damage model for cyclic loading of concrete structures," *Journal of Engineering Mechanics*, vol. 124, no. 8, pp. 892–900, 1998.

[23] J. Li, J. Y. Wu, and J. B. Chen, *Stochastic Damage Mechanics of Concrete Structures*, Science Press, Beijing, China, 2014.

[24] J. Li and X. D. Ren, "Recent developments on stochastic damage mechanics for concrete," *Journal of Building Structures*, vol. 35, no. 4, 2014.

[25] Y. W. Zhou and Y. F. Wu, "General model for constitutive relationships of concrete and its composite structures," *Composite Structures*, vol. 94, no. 2, pp. 580–592, 2012.

[26] A. A. Arab, *Finite Element Modeling of Pretensioned Concrete Girder: A Methodological Approach with Applications in Large Strands and End Zone Cracking*, Southern Illinois University, Edwardsville, IL, USA, 2012.

[27] American Concrete Institute, *Building Code Requirements for Structural Concrete (ACI 318-08) and Commentary*, American Concrete Institute, Farmington Hills, MI, USA, 2008.

[28] J. G. Nie and Y. H. Wang, "Comparison study of constitutive model of concrete in ABAQUS for static analysis of structures," *Engineering Mechanics*, vol. 30, no. 4, pp. 59–67, 2013.

[29] L. Wang, Y. F. Ma, W. Ding, J. Zhang, and Y. Liu, "Comparative study of flexural behavior of corroded beams with different types of steel bars," *Journal of Performance of Constructed Facilities*, vol. 29, no. 6, pp. 631–639, 2015.

[30] P. Kmiecik and M. Kaminski, "Modelling of reinforced concrete structures and composite structures with concrete strength degradation taken into consideration," *Archives of Civil and Mechanical Engineering*, vol. 11, no. 3, pp. 623–636, 2011.

[31] Z. Zhao and X. D. Jiang, *Monitoring and Diagnosis of Durability of Corroded Concrete Structure*, The Yellow River Water Conservancy Press, Zhengzhou, China, 2006.

[32] A. Neville, "Corrosion of reinforcement," *Concrete*, vol. 17, 1983.

[33] G. H. Xing and D. T. Niu, "Analytical model of flexural behaviour of corroded reinforced concrete beams," *Journal of Central South University (Science and Technology)*, vol. 45, no. 1, pp. 193–201, 2014.

[34] D. Coronelli and P. Gambarova, "Structural assessment of corroded reinforced concrete beams: modeling guidelines," *Journal of Structural Engineering*, vol. 130, no. 8, pp. 1214–1224, 2004.

[35] A. Ouglova, Y. Berthaud, F. Foct, M. François, F. Ragueneau, and I. Petre-Lazar, "The influence of corrosion on bond properties between concrete and reinforcement in concrete structures," *Materials & Structures*, vol. 41, no. 5, pp. 969–980, 2008.

[36] C. A. Apostolopoulos and V. G. Papadakis, "Consequences of steel corrosion on the ductility properties of reinforcement bar," *Construction and Building Materials*, vol. 22, no. 12, pp. 2316–2324, 2008.

[37] T. A. Söylev and R. François, "Corrosion of reinforcement in relation to presence of defects at the interface between steel and concrete," *Journal of Materials in Civil Engineering*, vol. 17, no. 4, pp. 447–455, 2005.

[38] W. L. Jin and J. Xia, "Influence of pitting corrosion on the bending capacity of reinforced concrete beams," *Building Structure*, vol. 39, pp. 100–102, 2009.

[39] X. H. Wang and X. L. Liu, "Modeling the flexural carrying capacity of corroded RC beam," *Journal of Shanghai Jiaotong University*, vol. 13, no. 2, pp. 129–135, 2008.

[40] X. Z. Lu, J. G. Teng, L. P. Ye, and J. J. Jiang, "Bond–slip models for FRP sheets/plates bonded to concrete," *Engineering Structures*, vol. 27, no. 6, pp. 920–937, 2005.

[41] W.-L. Qu and Y. Wang, "Investigation on force-bearing capacity of corroded reinforced concrete beam by using nonlinear finite element analysis," *Journal of Wuhan University of Technology*, vol. 29, no. 6, pp. 73–75, 2007.

[42] A. Kivell, A. Palermo, and A. Scott, "Complete model of corrosion degraded cyclic bond performance in reinforced concrete," *Journal of Structural Engineering*, vol. 141, no. 9, pp. 1–9, 2014.

[43] MC90 CEB-FIP Model Code, *Design of Concrete Structures*, British Standard Institution, London, UK, 1990.

[44] A. A. Almusallam, "Effect of degree of corrosion on the properties of reinforcing steel bars," *Construction and Building Materials*, vol. 15, no. 8, pp. 361–368, 2001.

[45] Y. Auyeung, P. Balaguru, and L. Chung, "Bond behavior of corroded reinforcement bars," *ACI Structural Journal*, vol. 97, no. 2, pp. 214–220, 2000.